Article

NIR-mediated Deformation from a CNT-based Bilayer Hydrogel

Shijun Long *, Chang Liu , Han Ren , Yali Hu , Chao Chen , YiWan Huang , Xuefeng Li *

Posted Date: 18 March 2024

doi: 10.20944/preprints202403.0974.v1

Keywords: temperature-responsive hydrogel; particle-double network; photothermal conversion; actuator; carbon nanotubes

Article

NIR-Mediated Deformation from a CNT-Based Bilayer Hydrogel

Shijun Long [1,2,3,*], Chang Liu [1], Han Ren [1], Yali Hu [1], Chao Chen [4], Yiwan Huang [1,2] and Xuefeng Li [1,2,3,*]

[1] Hubei Provincial Key Laboratory of Green Materials for Light Industry, Hubei University of Technology, Wuhan 430068, China; liuchang9708@163.com (C.L.); renhann@126.com (H.R.); hu_yali1@163.com (Y.H.); yiwanhuang@hbut.edu.cn (Y.H.);

[2] Hubei Longzhong Laboratory, Xiangyang, 441000, PR China

[3] New Materials and Green Manufacturing Talent Introduction and Innovation Demonstration Base, Hubei University of Technology, Wuhan, 430068, PR China

[4] Hubei Key Laboratory of Polymer Materials, Hubei University, 430062, Wuhan, PR China; chenchao@hubu.edu.cn(C.C.);

* Correspondence: longshijun.hp@163.com (S.L.); li_xf@mail.hbut.edu.cn (X.L.)

Abstract Shape-shifting polymers are widely used in various fields such as intelligent switches, soft robots and sensors, which require both multiple stimulus response functions and qualified mechanical strength. In this study, a novel near infrared light (NIR) responsible shape-shifting hydrogel system was designed and fabricated, through embedding vinylsilane modified carbon nanotubes (CNTs) into particle-double network (P-DN) hydrogels by micellar copolymerization. The dispersed brittle Poly(sodium 2-acrylamido-2-methylpropane-1-sulfonate) (PNaAMPS) network of the microgels can serves as sacrificial bonds to toughen the hydrogels, and the CNTs endow it NIR photothermal conversion ability. The results show that the CNTs embedded P-DN hydrogels present excellent mechanical strength, i. e. fracture strength of 312 kPa and fracture strain of 357%. Moreover, an asymmetric bilayer hydrogel, where the active layer contains CNTs, can achieve 0°–110° bending deformation within 10 min under NIR irradiation and can realise complex deformation movement. This study provides a theoretical and experimental basis for the design and manufacture of photoresponsive soft actuators.

Keywords: temperature-responsive hydrogel; particle-double network; photothermal conversion ; actuator; carbon nanotubes

1. Introduction

Stimuli-responsive hydrogels, also known as smart hydrogels, are materials that respond to stimuli in the external environment and undergo considerable changes in colour [1–3], volume [4] and mechanical properties [5]. According to different stimulus response modes, they can be roughly divided into temperature-responsive hydrogels [6], electrical responsive hydrogels [7], light responsive hydrogels [8,9], magnetic responsive hydrogels [10–12] and chemical responsive hydrogels [13,14]. Because of these characteristics, they have various applications in intelligent switches [15,16], artificial muscles [17,18], soft robots [19], shape-memory materials and other fields [20–23]. The use of temperature-responsive hydrogels is a relatively mature and simple method. It is a type of hydrogel material that can produce phase changes in the process of temperature change, usually with a lower critical transition temperature (LCST) or an upper critical transition temperature. As a typical representative of a temperature responsive hydrogel, Poly (N-isopropyl acrylamide)(PNIPAM) hydrogel has attracted much attention because of its LCST (32°C), which is close to human body temperature [24]. At temperatures below the LCST, the polymer chains of PNIPAM tend to form hydrogen bonds with water molecules, which are in a stretched state, causing the hydrogel to swell. At temperatures above the LCST, the polymer chains of PNIPAM are prone to forming hydrogen bonds on their own, expelling water and causes the polymer network to collapse.

 doi:10.20944/preprints202403.0974.v1

However, NIPAM hydrogels have only a single function; therefore, they have a narrow application range and are often restricted in complex environments. To overcome this, a feasible strategy is to use multiple functional substances to achieve the multiple stimulus responsiveness of hydrogels.

By contrast, light, as a noncontact and remotely controllable stimulus, can switch between two-dimensional and three-dimensional spatial scales and can be easily controlled in the temporal dimension by turning on and off the light source. In addition, light energy is adjusted by its own properties (e.g. wavelength and intensity), commonly including near-infrared (NIR), visible (vis) light and ultraviolet light [25–27]. Light stimulation can change the physical and chemical properties of a hydrogel, primarily by changing its network structure. According to the action mechanism, the effects of light stimulation on hydrogels can be divided into three categories. First, light can directly cause the formation and breaking of chemical bonds and change the cross-link density of hydrogels. Moreover, light of a specific wavelength can isomerise corresponding photosensitive molecules, such as the cis trans isomerisation of azobenzene and the open and closed loops of spiropyran, which can cause sol–gel transitions or change the swelling performance of the hydrogel. In addition, nanomaterials with photothermal properties, such as carbon nanotubes (CNTs) and graphene, can be introduced into hydrogel systems. These materials absorb light energy and convert it into thermal energy, thereby triggering thermally responsive hydrogels.

Herein, we modified CNTs using a silane coupling agent, introduced reactive groups to the surface of CNTs, and prepared CNT composite hydrogels. Because of the existence of NIPAM and CNTs, hydrogels can respond to thermal and light stimuli. Combined with a particle-double network (P-DN) hydrogel strategy, it also has good mechanical properties. Furthermore, we prepared a hydrogel actuator using a photothermal conversion function with an asymmetric bilateral structural design, which can realise rapid bending deformation under infrared light stimulation.

2. Experimental Section

2.1. Materials

N-isopropyl acrylamide (NIPAM, 98%) and methyl acrylate (MA, 98.5%) were supplied by Shanghai Macklin Biochemical Co., Ltd. Hydroxylated multiwalled carbon nanotubes (95%), Triethoxyvinylsilane (TEVS, 97%) and N,N,N′,N′-tetramethylethylenediamine (TEMED, 99%) were supplied by Shanghai Aladdin Bio-Chem Technology Co., Ltd. Ethanol absolute (analytical reagent), benzene (analytical reagent), Tween 80 (chemically pure), ammonium persulfate (APS, analytical reagent) and N,N′-methylene diacrylamide (MBAA, chemically pure) were supplied by Sinopharm Chemical Reagent Co., Ltd. Poly(sodium 2-acrylamido-2-methylpropane-1-sulfonate) (PNaAMPS) was prepared according to the method used in our previous study [28].

2.2. Modification of CNTs

The silane coupling agent (Triethoxyvinylsilane) is entangled and coated on the surface of the CNTs after refluxing, hydrolysis and condensation in water. The experimental process is as follows. Hydroxylated multiwalled CNTs (1.0 g) were added to deionised water (200 mL) in a beaker, which was then placed in an ultrasonic cell breaker and sonicated for 30 min under ice-water bath conditions at 270 W. After adding Triethoxyvinylsilane (5.65 g) and anhydrous ethanol (40 mL), the mixture was placed in the ultrasonic cell breaker and sonicated. After ultrasonic dispersion, the CNT diversions were poured into a 500-mL three-necked flask in an oil bath at 88°C for 24 h. The speed of the mechanical stirrer was adjusted to 280 rpm. After the reaction, the product was filtered using a Buchner funnel. The reaction product was first rinsed with a large amount of benzene and then with a large amount of ethanol. When no liquid droplets were visible on the surface of the CNT mixture, the product was placed onto aluminium foil and dried in a vacuum drying oven at 100°C for 24 h.

2.3. Preparation of the Hydrogel

The photothermal PNaAMPS/P(NIPAM-co-MA)/CNT hydrogels were prepared from a precursor aqueous solution containing 2.0-mol L^{-1} NIPAM, 10 wt% hydrophobic monomer MA,

 doi:10.20944/preprints202403.0974.v1

Tween 80 emulsifier (1.0 wt% of water), the photothermal component CNTs (0.00–0.20 wt% of the total monomer), 0.1 mol% of the chemical cross-linker MBAA and 0.1 mol% redox initiators. Initiators (APS and TEMED) were added to the solution at room temperature to form a mixed aqueous solution. The solution was transferred into a reaction cell (100 mm x 100 mm) comprising a pair of parallel glass plates and polyester films separated by a hollow silicone-rubber spacer ≈1 mm thick. The solution was polymerised in a refrigerator at 5°C for 12 h to form PNaAMPS/P(NIPAM-co-MA)/CNTs hydrogel.

2.4. Fabrication of the Bilayer Hydrogel

The upper hydrogel layer (active layer) containing the CNTs was prepared according to the method described in Section 2.3. After polymerisation, the prepolymer solution of the second hydrogel layer (negative layer) was added to the first hydrogel layer. The second layer of the hydrogel prepolymer solution did not contain CNTs, and the remaining preparation steps were identical to those used for the first layer described in Section 2.3.

2.5. Characterisation of Hydrogels

2.5.1. Fourier-Transform Infrared Spectrometry

The samples were dried in a 90°C vacuum drying oven for 24 h and then ground with an appropriate amount of potassium bromide powder to obtain a fine and uniform powder. Before testing, the sample and potassium bromide powder were placed in a 90°C vacuum drying oven for 30 min. Fourier-transform infrared spectrometry (Bruker, Tensor II) was undertaken between 4000 and 500 cm^{-1}.

2.5.2. Raman Spectrometry

The low-frequency analysis of gel samples was performed using a micro confocal Raman spectrometer (XploRA PLUS) with a 532-nm argon ion laser as the light source. The Raman spectroscopy measurements were conducted at room temperature with a displacement range of 200–3000 cm^{-1}.

2.5.3. Field-Emission Scanning Electron Microscopy

The microstructure of the hydrogel was observed using field-emission scanning electron microscopy (FESEM; SU8010; Hitachi Limited Co., Hitachi, Japan). Specifically, the sample was frozen and fractured in liquid nitrogen, followed by freeze drying for 48 h. Before FESEM characterisation, a thin layer of gold was applied to the fractured surface of the sample by sputtering. The acceleration voltage of FESEM was 5.0 kV.

2.5.4. Tensile Measurements

At room temperature, uniaxial tensile tests were performed with rectangular strips (30 mm × 5 mm) of the samples using a universal tensile testing machine (CMT6103; MTS Co. Ltd., Shanghai, China) equipped with a 1-kN load cell at a constant stretching velocity of 100 mm min^{-1}. The elastic modulus E was calculated from the slope of the initial linear region of the stress–strain curve (within the range of 5%–10%). The extension work was calculated from the area under the stress–strain curve to the fracture of the uncut sample. The nominal stress σ was calculated from the tensile force and the initial cross-sectional area of the undeformed sample. The strain rate ε was defined as the ratio of the stretching speed to the original gauge length. Unless otherwise specified, three measurements were performed for each sample.

 doi:10.20944/preprints202403.0974.v1

2.5.5. X-ray Photoelectron Spectrometry

To accurately analyze the chemical composition and elemental chemical state of the sample, an X-ray photoelectron spectrometer (PHI-5000 VP-Ⅲ; ULVAC JAPAN LTD) was used in the experiment. we use monochromatic X-ray, K-α Aluminum micro focusing light source and 0.60 eV photon energy. The sputtering source forms a grating on the surface of the sample with a rectangle of 1.40mm x 1.40mm

2.5.6. Equilibrium Swelling Ratio

The swelling properties of the hydrogels were measured over a wide temperature range. First, the hydrogel samples were placed in deionised water and maintained under various temperatures to reach swelling equilibrium. They were then removed from the deionised water and their surfaces wiped with filter paper before measuring their weight (W_s). Finally, the samples were fully dried in an oven at 100°C to determine their weight after drying (W_d). The equilibrium swelling ratio (ESR) was determined as follows:

$$ESR(wt\%) = \frac{W_s - W_d}{W_d} \times 100\%.$$

2.5.7. Photothermal Conversion

The swelling-equilibrated hydrogel samples were cut into discs with 1-cm diameters, placed on glass slides and irradiated with a 980-nm infrared laser maintained at 2.0 W. The temperature changes in the samples were measured using an infrared camera (FLIR 5L).

3. Results and Discussion

Here, we report the fabrication of a hydrogel with photothermal conversion and deformation abilities. As shown in Scheme 1, the hydrogel contains NIPAM, MA, PNaAMPS, MBAA, Tween80, APS, TEMED and modified CNTs. Each of these has different functions in the gel: (i) NIPAM and MA polymerize to form a continuous phase, while PNaAMPS microgel acts as a dispersion phase, forming a particle-double network (P-DN) structure and dispersing in the hydrogel matrix; (ii) the MBAA is the cross-linker; (iii) the APS and TEMED are the redox initiation systems and (iv) Tween 80 is an emulsifier. In this hydrogel matrix, CNTs conduct photothermal conversion and provide mechanical enhancement. As a thermal responsive component, NIPAM can synergistically act with CNTs to achieve photoresponsive deformation. Photothermal agent carbon nanotubes convert light energy into heat energy, and the PNIPAM component in P-DN hydrogel undergoes phase transformation and contraction when the temperature rises to LCST To add CNTs to the hydrogel matrix to achieve an effective and stable connection, we used a silane coupling agent to modify the surface of carbon nanotubes introducing double bonds on its surface to achieve covalent bonding.

 doi:10.20944/preprints202403.0974.v1

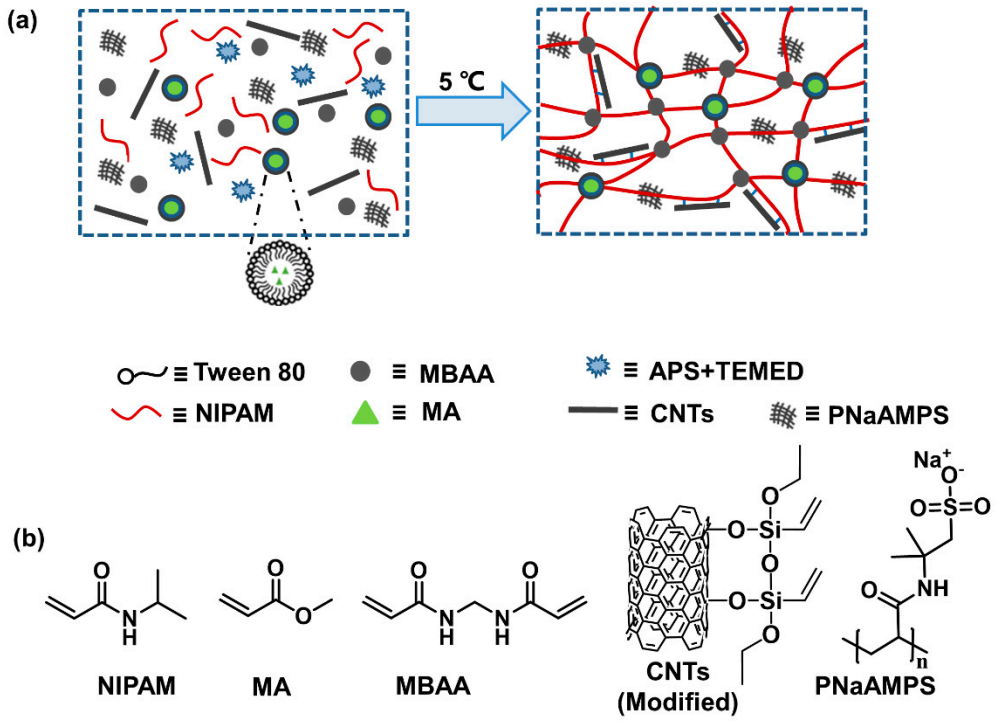

Scheme 1. Preparation of the PNaAMPS/P(NIPAM-co-MA)/CNT hydrogel. (a) Hydrogel synthesis mechanism and (b) the structural formula of the main components.

3.1. Characterisation of the Microstructure (Infrared Spectrum, Raman Spectrum, X-ray Photoelectron Spectroscopy and SEM)

Figure 1a is a schematic of the surface modification of the CNTs using a silane coupling agent (Triethoxyvinylsilane). According to the Raman spectra in Figure 1b, before and after modification of the CNTs, the G peak at 1590 cm^{-1} represents the six-membered carbon ring structure of the CNTs and the D peak at 1350 cm^{-1} represents defects in the structure. Therefore, the ratio of the intensity of the D peak to that of the G peak reflects the regularity of the six-membered carbon ring structure of the CNTs. Figure 1b shows that the six-membered carbon ring structure on the surface of the CNTs remains unchanged before and after modification, and the ratio of the D peak to the G peak remains largely unchanged. This is because the grafting reaction occurs on the CNT substituents rather than on the six-membered carbon rings. The infrared spectrum in Figure 1c shows that the hydroxyl absorption peak at 3440 cm^{-1} is weakened after modification by the silane coupling agent. This can be attributed to the decrease in hydroxyl groups on the surface of the CNTs after the silane coupling reaction. Simultaneously, characteristic Si–O–Si symmetric and antisymmetric stretching vibration peaks appear at 1032 cm^{-1} and 1106 cm^{-1}, respectively, indicating that the silane coupling agent is successfully grafted onto the surfaces of CNTs. The X-ray photoelectron spectroscopy spectrum in Figure 1d shows that during the modification process, the oxygen content in the CNT sample slightly increases, which is speculated to be caused by the introduction of the silane coupling agent's oxygen elements. In addition, after modification, the characteristic peak corresponding to the 2s and 2p orbital of Si appear(153 eV and 101 eV), indicating that the silane coupling agent was successfully branched onto the surface of the CNTs.

 doi:10.20944/preprints202403.0974.v1

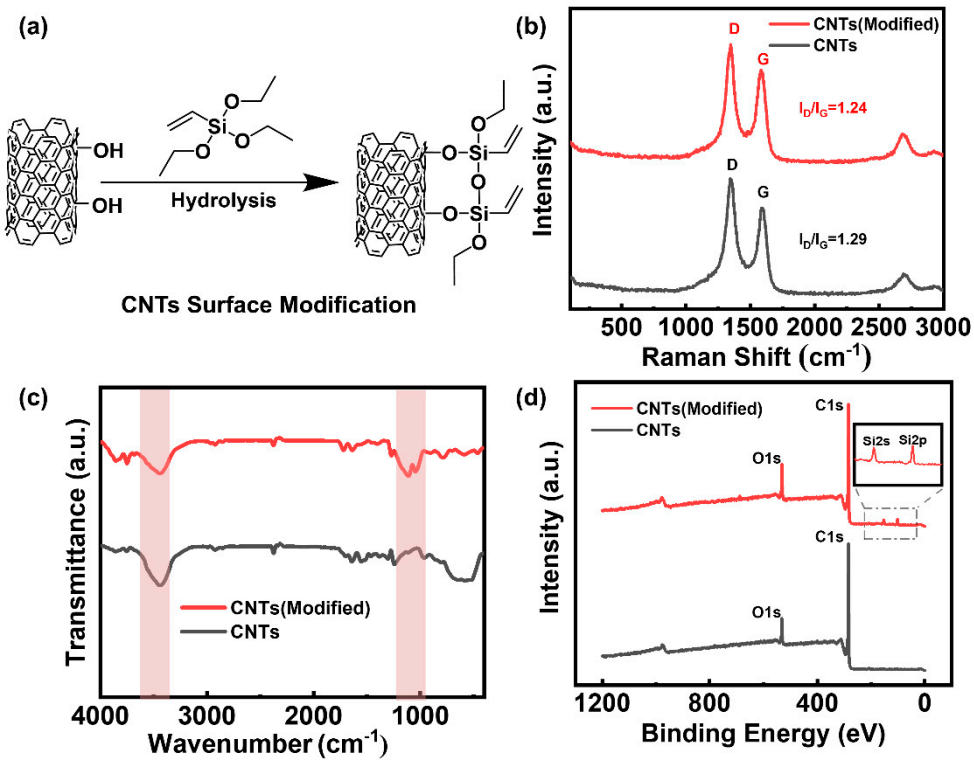

Figure 1. Microstructure characterisation of carbon nanotubes (CNTs) and modified CNTs. (a) Reaction principle of the silane coupling agent and the CNTs; (b) Raman spectroscopy of CNTs and modified CNTs; (c) infrared spectroscopy of CNTs and modified CNTs and (d) X-ray photoelectron spectroscopy of CNTs and modified CNTs.

Micromorphology analysis can explain the dispersion of nanofillers in nanocomposite hydrogels and the interaction between the filler and the matrix interface. As shown in Figure 2, the cross-sectional morphologies of the above hydrogels are typical porous structures and the network of the single-network gel is relatively loose, with large holes. Observed under the same magnification, compared with the single-network P(NIPAM-co-MA) hydrogel, the pores of the P-DN hydrogel are smaller and denser, which can be attributed to the denser polymer chain of the P-DN hydrogel. However, after the addition of CNTs to the double-network hydrogel, the polymer network becomes denser and the pore size gradually decreases, as seen in the SEM images in Figure 2. The possible reason is that carbon nanotubes are hydrophobic, which causes some water molecules to leave the hydrogel matrix, resulting in more dense hydrogel network.

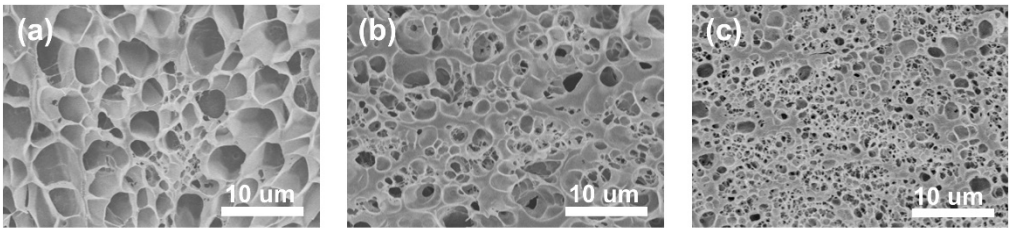

Figure 2. Scanning electron microscopy images of the hydrogels. (a) P(NIPAM-co-MA), (b) PNaAMPS/P(NIPAM-co-MA) and (c) PNaAMPS/P(NIPAM-co-MA)/CNTs.

 doi:10.20944/preprints202403.0974.v1

3.2. Tensile and Swelling Properties

According to the stress–strain curve in Figure 3a, the mechanical properties of the P-DN hydrogel with added PNaAMPS have been considerably improved and the fracture strength, fracture strain and Young's modulus have been considerably improved. According to Table 1, as a control group, the fracture strength of the P(NIPAM-co-MA) single-network hydrogel without CNTs was only 45 kPa, the fracture strain was 224% and the Young's modulus was 40 kPa, reflecting poor mechanical properties. The fracture strength, fracture strain and Young's modulus of the P-DN hydrogel with added PNaAMPS increased to 236 kPa, 324% and 47 kPa, respectively. This is attributed to the dieperse phase of the brittle PNaAMPS microgel breaking first, during which the network absorbs a large amount of energy and acts as a sacrificial bond, delaying the overall tensile fracture of the material[29,30]. Moreover, after adding a small number of CNTs to the P-DN hydrogel, the mechanical properties of the hydrogel improve slightly. When the amount of CNTs added was 0.15 wt%, the breaking strength, breaking elongation and Young's modulus reached 312 kPa, 335% and 79 kPa, respectively, which increased by 32.20%, 3.40% and 68.09% compared with the hydrogel without CNTs. As the concentration of CNTs further increases, the tensile properties of the sample begin to decrease. This is because when the content is low, the CNTs have a fibre-strengthening effect on the hydrogel matrix. When the content is increased, the CNTs are clustered together and are difficult to disperse evenly; therefore, they form defects in the matrix.

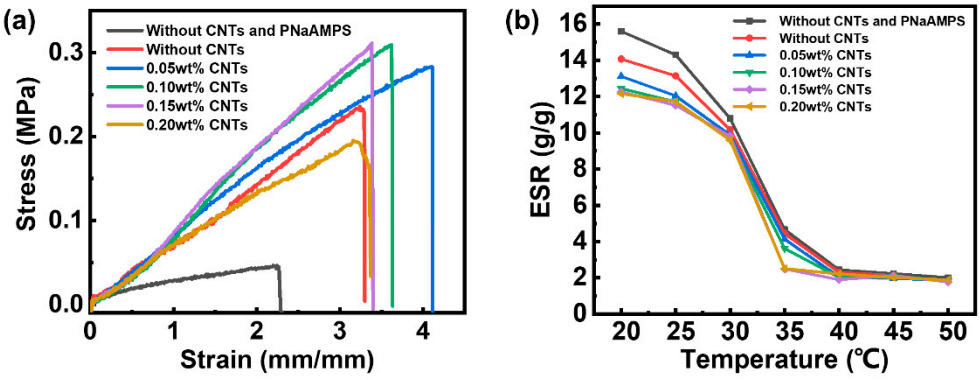

Figure 3. Mechanical and swelling properties of hydrogels with PNaAMPS/P(NIPAM-co-MA)/CNTs, PNaAMPS/P(NIPAM-co-MA) and P(NIPAM-co-MA). (a) Stress–strain curves and (b) equilibrium swelling ratio–temperature curves.

Figure 3b shows that the ESR–temperature curves of hydrogels with various CNT contents follow nearly the same variation law. Under low-temperature conditions, all the hydrogels show swelling behaviour. The equilibrium swelling ratio of P-DN hydrogels was lower than that of single-network hydrogels (control group). Because the polymer chain density of P-DN hydrogels are higher than that of single-network hydrogel, which hinder the swelling process of materials. And the curve shows that at 20°C, compared with P-DN hydrogel without CNTs, the equilibrium swelling ratio of the P-DN hydrogel containing CNTs decreases by 6.5%–13.6%. This can be attributed to the hydrophobic characteristics of the CNTs, which provide an explanation for the enhanced mechanical properties. When water molecules leave the hydrogel matrix, the equilibrium swelling ratio decreases and the polymer chain density increases, eventually leading to an increase in strength. At high temperatures, the equilibrium swelling ratio of all the hydrogels decrease considerably, which manifests as shrinkage due to water loss. In the range of 30°C–35°C, there is a transition from hydrophilicity to hydrophobicity. The temperature response behaviour of the hydrogel is attributed to the PNIPAM component in the hydrogel. This transition means that PNIPAM is a typical LCST-type polymer. At low temperatures, PNIPAM molecules form hydrogen bonds with water molecules and the macroscopic performance is water-absorption swelling. As the temperature increases, the hydrogen bonds between the water molecules and the PNIPAM molecules gradually break and most

 doi:10.20944/preprints202403.0974.v1

of the water molecules leave the interior of the hydrogel, which is reflected in the macroscopic shrinkage of the hydrogel.

Table 1. Comparison of the mechanical properties of all hydrogel types.

Sample	σ (kPa)	ε (%)	W (kJ m^{-3})	E (kPa)
Without CNTs and	45 ± 9	224 ± 29	65 ± 27	40 ± 9
PNaAMPS	236 ± 16	324 ± 18	396 ± 39	47 ± 3
Without CNTs	282 ± 11	405 ± 13	644 ± 21	77 ± 11
0.05 wt% CNTs	309 ± 19	357 ± 11	576 ± 14	73 ± 10
0.10 wt% CNTs	312 ± 20	335 ± 26	507 ± 25	79 ± 12
0.15 wt% CNTs	195 ± 7	310 ± 20	361 ± 37	69 ± 7
0.20 wt% CNTs				

3.3. Photothermal Conversion Test

Figure 4a and 4b shows that all hydrogels with added CNTs exhibited photothermal conversion. With longer periods of NIR light irradiation, the surface temperature of the hydrogel with added CNTs rapidly rises. With the increase in CNT content, the hydrogel surface temperature rise rate increases. As a control group, the surface temperature of the hydrogel without CNTs increased only slightly. This is attributed to the photothermal conversion effect of CNTs. Compared with metal and inorganic materials, carbon-based materials, such as CNTs, have been selected as superior photothermal conversion materials because of their inherent excellent properties: they have extremely high light absorption in the vis and NIR bands and a large number of conjugated six-membered carbon ring structures, which facilitate excited-state electron migration to transfer heat. In addition, because of the excellent thermal conductivity of CNTs, heat can be quickly transferred to the hydrogel matrix. When the amount of CNTs added reaches 0.20 wt%, there is no significant improvement in the photothermal conversion performance. The possible reason is that when the concentration of CNTs is high, the ability to absorb light tends to saturate(Figure S1). Therefore, we selected the sample with 0.20 wt% CNTs for subsequent research. Simultaneously, the hydrogel changes from transparent to opaque and exhibits a certain degree of water loss after being irradiated with near infrared light, which also confirms the LCST properties of PNIPAM(Figure S2). Furthermore, we evaluated the recyclability of the photothermal conversion effect of hydrogels. The hydrogel added with CNTs was irradiated under NIR for 5min, and then the light was off to cool the hydrogel to near room temperature. The surface temperature of the hydrogel can still reach 64°C after this process is repeated five times(Figure S3)

As a photothermal agent in hydrogels, photothermal conversion is a crucial characteristic. Therefore, the photothermal conversion performance of the carbon nanotubes was evaluated.

We dispersed CNTs in water and then irradiated them with a 980-nm NIR laser of 2 Wcm^{-2}. We used pure water as the negative control group. As shown in Figure 4c, the temperature of the CNT solution rapidly increases under NIR radiation. After 300 s of irradiation, the temperature of the CNT solution was 53.9°C (an increase of 24°C). By contrast, the temperature of the pure water is 40.3°C (an increase of only 10.4°C). After 300 s of irradiation, the NIR laser was turned off and the reducing temperature was recorded for 900 s. The temperature change (ΔT) response to the NIR laser during 1200 s is shown in Figure 4c. Linear time data versus −ln (θ) was obtained from the cooling period of the NIR lasers. This relationship is shown in Figure 4b. The photothermal conversion efficiency of CNTs (η) was calculated according to the following equation [31]:

$$\eta = \frac{hA\left(\Delta T_{max,mix} - \Delta T_{max,H_2O}\right)}{I\left(1-10^{-A_\lambda}\right)},$$

where h is the heat transfer coefficient, A is the surface area of the container, $\Delta T_{max,mix}$ and $\Delta T_{max,H2O}$ are the temperature changes of the carbon nanotube aqueous dispersion and solvent (water), respectively, at the maximum steady-state temperature, I is the laser power and A_λ is the absorbance of the carbon nanotube aqueous dispersion at 980 nm. For detailed information on the calculations,

 doi:10.20944/preprints202403.0974.v1

please refer to the reported literature[31,32]. According to this equation, we calculate the η of CNT to be approximately 21.73%.

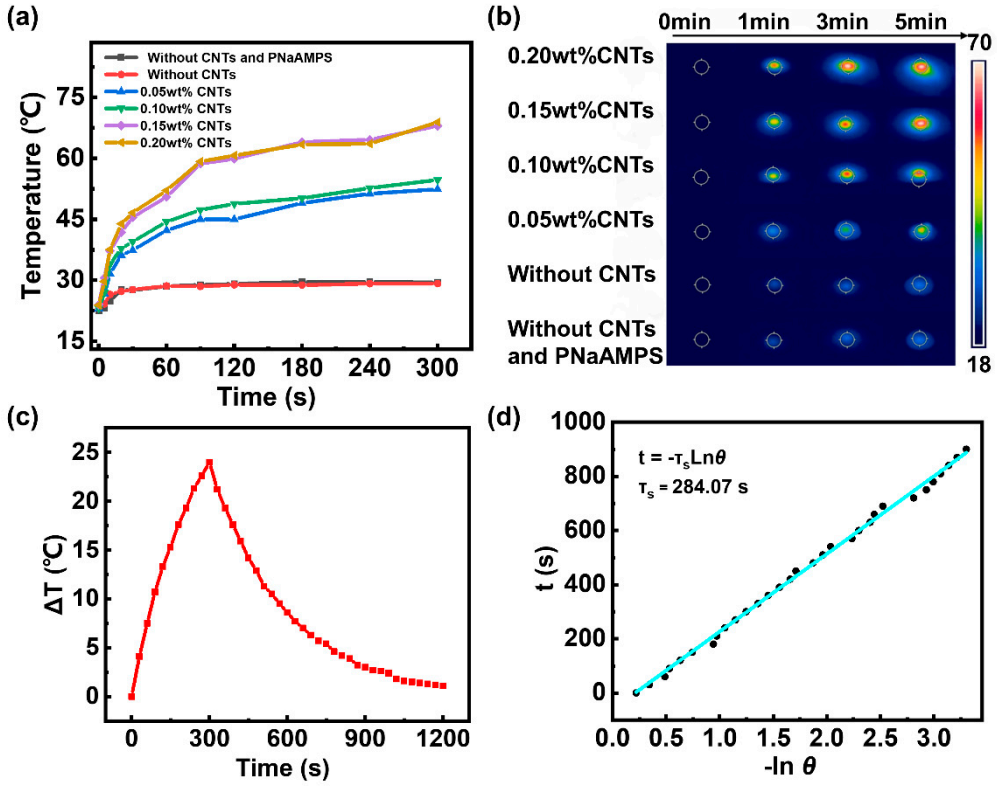

Figure 4. Photothermal conversion properties of hydrogels with PNaAMPS/P(NIPAM-co-MA)/CNTs, PNaAMPS/P(NIPAM-co-MA) and P(NIPAM-co-MA). (a) Temperature–time curves, (b) infrared thermal images of hydrogels under infrared light, (c) temperature change (ΔT) of PNaAMPS/P(NIPAM-co-MA)/CNTs hydrogel during NIR irradiation and NIR off(d) Linear time data versus-ln (θ) fitting curves of PNaAMPS/P(NIPAM-co-MA)/CNTs hydrogel(obtained from the cooling period of NIR laser off).

3.4. Bending and Complex Deformation of Hydrogels

To prepare the photoresponsive hydrogel actuators, we designed hydrogels with a bilayer structure. The structure of the hydrogel is shown in Figure 5a. The preparation method for the photoactive layer was the same as that used for the single-layer hydrogel. The second layer (negative layer) of the bilayer hydrogel does not contain CNTs, and the remaining steps are the same as those used for the first layer. When the NIR laser is on, the temperature of the active layer rapidly rises and the PNIPAM in the matrix undergoes phase transition and shrinkage owing to dehydration. Owing to shrinkage of the active layer and swelling of the negative layer, the bilayer hydrogel bends towards the active layer. Using an infrared laser to illuminate the centre of the active-layer hydrogel, we recorded the changes in hydrogel bending angles (as shown in Figure 5a) with irradiation time. Figure 5b,c shows that when the control group (bilayer hydrogel without CNTs) was irradiated, the bending angle of the hydrogel sample changed very little. When the bilayer hydrogel with 0.20 wt% CNTs was exposed to the NIR laser, obvious bending deformation was observed. The bending angles of the bilayer hydrogel (0.20 wt% CNTs in the active layer) rapidly increased from 0° to 110° within 10 min. This reflects good photothermal conversion and deformation ability. Through cyclic experiments, it was found that this deformation process can be repeated at least eight times(Figure S4).

 doi:10.20944/preprints202403.0974.v1

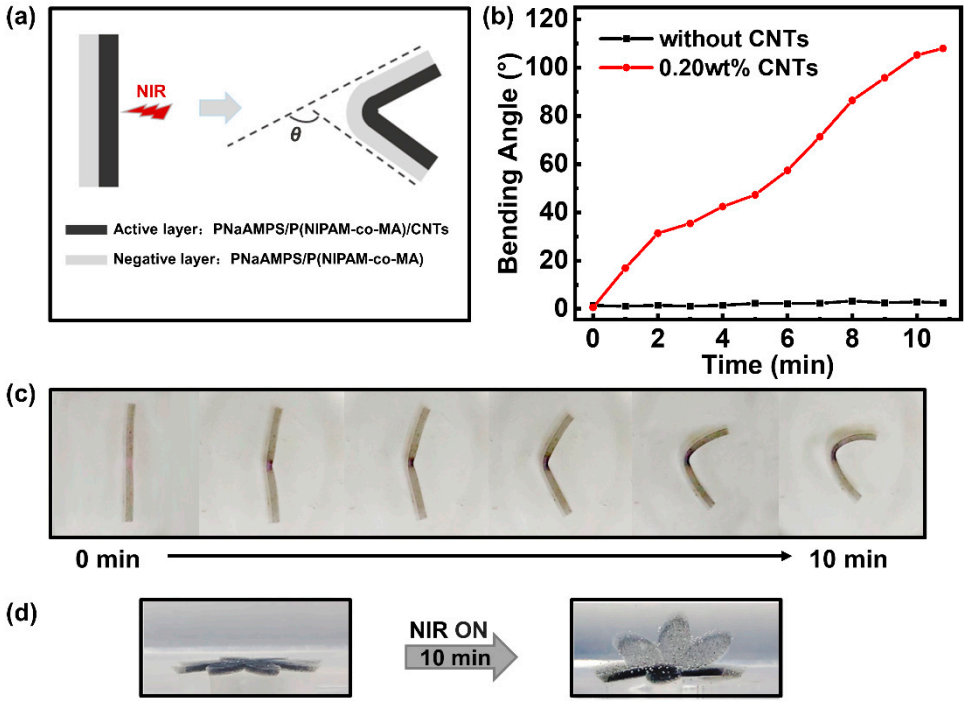

Figure 5. Deformation of PNaAMPS/P(NIPAM-co-MA)/CNTs hydrogel. (a) Schematic of the bending angle measurement, (b) bending angles of hydrogels, (c) images of the bending angles and (d) images of the complex deformation.

Based on the bending deformation, we designed more complex three-dimensional deformation experiments, such as the folding and opening of flower-shaped hydrogels. The bilayer hydrogel was cut into complex geometric shapes (like a flower with eight petals) with a plastic mould, irradiated with an infrared laser and deformation was observed, as shown in Figure 5d. The bilayer hydrogel changed from completely flat to slightly curved in about 5 min under infrared light irradiation and became completely folded like a flower after 10 min of continuous irradiation. After removing the infrared light for a certain period, the shape slowly recovered after deformation.

4. Conclusions

In this study, CNTs modified by silane coupling agent were successfully prepared and hydrogel actuator were fabricated on this basis. Fourier-transform infrared (FTIR) spectrometry and X-ray photoelectron spectrometry (XPS) indicated that the functional groups were successfully grafted onto the CNTs through hydrolysis and condensation reactions. The modified CNTs were then introduced into the hydrogel matrix. The photothermal conversion experiment showed that adding only a small amount of CNTs can endow the hydrogel with photothermal conversion ability. The tensile test results showed that the Microgel-Reinforced strategy can considerably enhance the mechanical properties of the hydrogel. To some extent, the introduction of CNTs can also improve the mechanical properties of the hydrogel. Then, using the bilayer structural design, a hydrogel actuator that could achieve deformation movement under infrared light irradiation was prepared. By studying the hydrogel photothermal actuator, we found that the actuator has good repeatability and stimuli responsiveness. This study provides a simple and convenient method for preparing CNT hydrogels and provides a theoretical and technical basis for the development of new hydrogel actuators.

Supplementary Materials: The following supporting information can be downloaded at the website of this paper posted on Preprints.org. Figure S1: Optical photos of the phase transition behavior of PNaAMPS/P(NIPAM-co-MA)/CNTs hydrogels under near-infrared light irradiation; Figure S2: Transmittance curve of all hydrogels(PNaAMPS/P(NIPAM-co-MA), PNaAMPS/P(NIPAM-co-MA)/CNTs and SN: P(NIPAM-

co-MA)); Figure S3: Cyclic reversible photothermal conversion behavior of PNaAMPS/P(NIPAM-co-MA)/CNTs hydrogels(Control group: PNaAMPS/P(NIPAM-co-MA) hydrogel); Figure S4: Cyclic reversible bending behavior of bilayer hydrogel(active layer: PNaAMPS/P(NIPAM-co-MA)/CNTs, negative layer: PNaAMPS/P(NIPAM-co-MA)) under infrared light irradiation.

Author Contributions: Conceptualization, X.L. and S.L.; methodology and investigation, S.L. and C.L.; formal analysis, C.L. and S.L.; Scanning electron microscopy imaging measurements, Y.H.; tensile measurements, Y.H. and H.R.; writing—original draft preparation, C.L.; writing—review and editing, S.L. and C.C.; discussion of experiments, C.C., X.L. and S.L. All authors have read and agreed to the published version of the manuscript.

Funding: This research was supported by the National Natural Science Foundation of China (Contract no. 52073083 and 51603065).

Institutional Review Board Statement: Not applicable.

Data Availability Statement: Not applicable.

Acknowledgments: Not applicable.

Conflicts of Interest: The authors declare no conflict of interest.

References

1. Willner, I. Stimuli-controlled hydrogels and their applications. *Acc. Chem. Res.* **2017**, *50*, 657–658.
2. Zhao, Y.; Xuan, C.; Qian, X.; Alsaid, Y.; Hua, M.; Jin, L.; He, X. Soft phototactic swimmer based on self-sustained hydrogel oscillator. *Sci. Robot.* **2019**, *4*, eaax7112.
3. Huan, H.; Xin, C.; Zhimin, M.; Rint, P.; Sibesma, Z.M., et al. Polymer mechanochromism from force-tuned excited-state intramolecular proton Transfer. *J. Am. Chem. Soc*. **2022**, *144*, 9971–9979.
4. Swift, T.; Swanson, L.; Geoghegan, M.; Rimmer, S. The pH-responsive behaviour of poly(acrylic acid) in aqueous solution is dependent on molar mass. *Soft Matter* **2016**, *12*, 2542–2549.
5. Montero de Espinosa, L.M.; Meesorn, W.; Moatsou, D.; Weder, C. Bioinspired polymer systems with stimuli-responsive mechanical properties. *Chem. Rev.* **2017**, *117*, 12851–12892.
6. Zheng, D.; Wang, K.; Bai, B.; Hu, N.; Wang, H.L. Swelling and glyphosate-controlled release behavior of multi-responsive alginate-g-P(NIPAm-co-NDEAm)-based hydrogel. *Carbohydr. Polym*. **2022**, *182*, 119113.
7. Lim, H.L.; Hwang, Y.; Kar, M.; Varghese, S. Smart hydrogels as functional biomimetic systems. *Biomater. Sci.* **2014**, *2*, 603-618.
8. Wang, L.; Li, Q. Stimuli-directing self-organized 3D liquid-crystalline nanostructures: from materials design to photonic applications. *Adv. Funct. Mater.* **2016**, *26*, 10–28.
9. Leistner, A.L.; Kistner, D.G.; Fengler, C.; Pianowski, Z.L. Reversible photodissipation of composite photochromic azobenzene-alginate supramolecular hydrogels. *RSC Adv*. **2022**,*12*, 4771-4776.
10. Ma, C.; Le, X.; Tang, X.; He, J.; Xiao, P.; Zheng, J.; Xiao, H.; Lu, W.; Zhang, J.; Huang, Y.; Chen, T. A multiresponsive anisotropic hydrogel with macroscopic 3D complex deformations. *Adv. Funct. Mater.* **2016**, *26*, 8670–8676.
11. Goodrich, R.; Tai, Y.; Ye, Z.Y.; Yin, Y.D.; Nam, J.A Magneto-Responsive Hydrogel System for the Dynamic Mechano-Modulation of Stem Cell Niche. *Adv. Mater*. **2023**, *33*, 12, 2211288.
12. Shu, Z.; Cao, Q.L.; Muhammad, U.; Zhang, T.Y.; J, W.X.; Chen, J.; Liu, Cong.; Wei, Y. Fabrication of high-strength magnetically responsive hydrogels by synergistic salting-out and freezing–thawing and application of their shape deformation and swimming. *Polym. Eng. Sci*. **2023**, *63*, 5, 1567-1578.
13. Yang, J.; Zhu, Z.Y.; Zhang, J.Z.; Chen, C.H.; Lei, Z.Y.; Li, L.Y.; Feng, Z.H.; Su, X. pH-Responsive polyethyleneimine hydrogel based on dynamic covalent bonds. *J. Polym. Res*. **2023**, *30*, 96.
14. Xiao, S.; Yang, Y.; Zhong, M.; Chen, H.; Zhang, Y.; Yang, J.; Zheng, J. Salt-responsive bilayer hydrogels with pseudo-double-network structure actuated by polyelectrolyte and antipolyelectrolyte effects. *ACS Appl. Mater. Interfaces* **2017**, *9*, 20843–20851.
15. Ma, C.; Lu, W.; Yang, X.; He, J.; Le, X.; Wang, L.; Zhang, J.; Serpe, M.J.; Huang, Y.; Chen, T. Bioinspired anisotropic hydrogel actuators with on-off switchable and color-tunable fluorescence behaviors. *Adv. Funct. Mater*. **2018**, *28*, 1704568.
16. Zhang, C.L.; Cao, F.H.; Wang, J.L.; Yu, Z.L.; Ge, J.; Lu, Y.; Wang, Z.H.; Yu, S.H. Highly stimuli-responsive au nanorods/poly(N-isopropylacrylamide) (PNIPAM) composite hydrogel for smart switch. *ACS Appl. Mater. Interfaces* **2017**, *9*, 24857–24863.

 doi:10.20944/preprints202403.0974.v1

17. Mirvakili, S.M.; Hunter, I.W. Artificial muscles: mechanisms, applications, and challenges. *Adv. Mater.* **2018**, *30*, 1704407.
18. Oveissi, F.; Fletcher, D.F.; Dehghani, F.; Naficy, S.Tough hydrogels for soft artificial muscles. *Mater. Des.* **2021**, *203*, 109609.
19. Park, C.S.; Kang, Y.W.; Na, H.; Sun, J.Y. Hydrogels for bioinspired soft robots. *Prog. Polym. Sci.* **2024**, *150*, 101791.
20. Han, Y.J.; Bai, T.; Liu, W.G. Controlled heterogeneous stem cell differentiation on a shape memory hydrogel surface. *Sci, Rep.* **2014**, *4*, 5815.
21. Shang, J.J.; Le, X.X.; Zhang, J.W.; Chen, T.; Theato, P. Trends in polymeric shape memory hydrogels and hydrogel actuators. *Polym. Chem.* **2019**, *10*, 1036-1055.
22. Wang, L.; Jian, Y.; Le, X.; Lu, W.; Ma, C.; Zhang, J.; Huang, Y.; Huang, C.F.; Chen, T. Actuating and memorizing bilayer hydrogels for a self-deformed shape memory function. *Chem. Commun.* **2018**, *54*, 1229–1232.
23. Stoychev, G.; Zakharchenko, S.; Turcaud, S.; Dunlop, J.W.C.; Ionov, L. Shape-programmed folding of stimuli-responsive polymer bilayers. *ACS Nano* **2012**, *6*, 3925–3934.
24. Din, M.I.; Khalid, R.; Akbar, F.; Ahmad, G.; Najeeb, J.; Nisa Hussain, Z.U.N. Recent progress of poly(N-isopropylacrylamide) hybrid hydrogels: synthesis, fundamentals and applications-review. *Soft Matter* **2018**, *16*, 228–247.
25. Thérien-Aubin, H.; Wu, Z.L.; Nie, Z.; Kumacheva, E. Multiple shape transformations of composite hydrogel sheets. *J. Am. Chem. Soc.* **2013**, *135*, 4834–4839.
26. Kim, D.; Lee, H.S.; Yoon, J. Highly bendable bilayer-type photo-actuators comprising of reduced graphene oxide dispersed in hydrogels. *Sci. Rep.* **2016**, *6*, 20921.
27. Kim, D.; Kim, H.; Lee, E.; Jin, K.S.; Yoon, J. Programmable volume phase transition of hydrogels achieved by large thermal hysteresis for static-motion bilayer actuators. *Chem. Mater.* **2016**, *28*, 8807-8814.
28. Long, S.; Huang, J.; Xiong, J.; Liu, C.; Chen, F.; Shen, J.; Huang, Y.; Li, X. Designing MultistimuliResponsive Anisotropic Bilayer Hydrogel Actuators by Integrating LCST Phase Transition and Photochromic Isomerization. *POLYMERS-BASEL*. **2023**, *15*, 786.
29. Hu, J.; Kurokawa, T.; Nakajima, T.; Sun, T.L.; Suekama, T.; Wu, Z.L.; Liang, S.L.; Gong, J.P. High Fracture Efficiency and Stress Concentration Phenomenon for Microgel-Reinforced Hydrogels Based on Double-Network Principle. *Macromolecules* **2012**, *45*, 23, 9445–9451.
30. Hu, J.; Kurokawa, T.; Nakajima, T.; Wu, Z.L.; Liang, S.L.; Gong, J.P. Fracture Process of Microgel-Reinforced Hydrogels under Uniaxial Tension. *Macromolecules* **2014**, *47*, 11, 3587–3594.
31. Roper, D.K.; Ahn, W.; Hoepfner, M. Microscale heat transfer transduced by surface plasmon resonant gold nanoparticles. *J. Phys. Chem. C* **2007**, *111*, 9, 3636-3641.
32. Wang, X.; Liu, X.H.; Ma, Z.Y.; Mu, C.L.; Li, W. Photochromic and photothermal hydrogels derived from natural amino acids and heteropoly acids. *Soft Matter* **2021**, *17*, 10140